J|A|C|S ARTICLES

Published on Web 01/20/2009

Inefficient Crystal Packing in Chiral $[Ru(phen)_3](PF_6)_2$ Enables Oxygen Molecule Quenching of the Solid-State MLCT Emission

Kari A. McGee and Kent R. Mann*

Department of Chemistry, University of Minnesota, Minneapolis, Minnesota 55455

Received September 23, 2008; E-mail: krmann@umn.edu

Abstract: The molecular oxygen quenching of the solid-state emission from pure crystals of Δ-$Ru(phen)_3(PF_6)_2$, Λ-$Ru(phen)_3(PF_6)_2$, and racemic $Ru(phen)_3(PF_6)_2$ (phen = 1,10-phenanthroline) was studied by emission spectroscopy. Crystals of the pure enantiomers exhibit significant and nearly identical emission-intensity quenching [0.36(2) and 0.33(2), respectively] in the presence of air [where the fraction quenched is $(I_{nitrogen} - I_{air})/I_{nitrogen}$]; in comparison, the racemic compound shows a much lower value [0.05(2)]. The large difference in the quenching behavior is a result of major structural differences between the two chiral salts and the racemic salt. The chiral compounds crystallize in the space groups $P4_1$ and $P4_3$, respectively, with toluene and acetonitrile molecules in the lattice that can be partially removed to create void-space channels. These open channels allow the diffusion of oxygen molecules within the crystals and enable efficient emission quenching that is not possible in the closely packed racemic salt. Lifetime measurements, thermal gravimetric analysis, and single-crystal X-ray structure determinations support these conclusions.

Introduction

The sensing of molecular oxygen in the gas phase and water with optical sensors has generated considerable interest in the past 20 years because optical sensing offers several advantages over electrochemical detection (i.e., the Clark electrode).[1−5] Solid-state optical sensors have been developed by embedding emissive transition-metal complexes in polymeric,[3,6−23] zeolitic,[24,25] sol−gel,[26−30] or other[31−36] support materials that allow oxygen to diffuse to the emissive sites. The emission of the metal complex is quenched via energy transfer to the oxygen molecules, allowing detection. Specifically, sensors utilizing $Ru(bpy)_3^{2+}$ (bpy = 2,2′-bipyridine) derivatives as the lumiphore have been commercialized.[37] Unfortunately, in these systems,

(1) Ando, M. *TrAC, Trends Anal. Chem.* **2006**, *25*, 937.
(2) Demas, J. N.; DeGraff, B. A. *Coord. Chem. Rev.* **2001**, *211*, 317.
(3) Demas, J. N.; DeGraff, B. A.; Coleman, P. B. *Anal. Chem.* **1999**, *71*, 793A.
(4) Mills, A. *Platinum Met. Rev.* **1997**, *41*, 115.
(5) Zhao, Y.; Richman, A.; Storey, C.; Radford, N. B.; Pantano, P. *Anal. Chem.* **1999**, *71*, 3887.
(6) Amao, Y.; Okura, I. *Sens. Actuators, B* **2003**, *88*, 162.
(7) Demas, J. N.; DeGraff, B. A.; Xu, W. *Anal. Chem.* **1995**, *67*, 1377.
(8) Draxler, S.; Lippitsch, M. E.; Klimant, I.; Kraus, H.; Wolfbeis, O. S. *J. Phys. Chem.* **1995**, *99*, 3162.
(9) Ertekin, K.; Kocak, S.; Sabih Ozer, M.; Aycan, S.; Cetinkaya, B. *Talanta* **2003**, *61*, 573.
(10) Fuller, Z. J.; Bare, W. D.; Kneas, K. A.; Xu, W. Y.; Demas, J. N.; DeGraff, B. A. *Anal. Chem.* **2003**, *75*, 2670.
(11) Garcia-Fresnadillo, D.; Marazuela, M. D.; Moreno-Bondi, M. C.; Orellana, G. *Langmuir* **1999**, *15*, 6451.
(12) Hartmann, P.; Leiner, M. J. P.; Lippitsch, M. E. *Anal. Chem.* **1995**, *67*, 88.
(13) Huynh, L.; Wang, Z.; Yang, J.; Stoeva, V.; Lough, A.; Manners, I.; Winnik, M. A. *Chem. Mater.* **2005**, *17*, 4765.
(14) Kneas, K. A.; Demas, J. N.; Nguyen, B.; Lockhart, A.; Xu, W.; DeGraff, B. A. *Anal. Chem.* **2002**, *74*, 1111.
(15) Kneas, K. A.; Xu, W.; Demas, J. N.; DeGraff, B. A. *Appl. Spectrosc.* **1997**, *51*, 1346.
(16) McMurray, H. N.; Douglas, P.; Busa, C.; Garley, M. S. *J. Photochem. Photobiol., A* **1994**, *80*, 283.
(17) McNamara, K. P.; Li, X.; Stull, A. D.; Rosenzweig, Z. *Anal. Chim. Acta* **1998**, *361*, 73.
(18) Mills, A. *Analyst* **1998**, *123*, 1135.
(19) Morin, A. M.; Xu, W.; Demas, J. N.; DeGraff, B. A. *J. Fluoresc.* **2000**, *10*, 7.
(20) Navarro-Villoslada, F.; Orellana, G.; Moreno-Bondi, M. C.; Vick, T.; Driver, M.; Hildebrand, G.; Liefeith, K. *Anal. Chem.* **2001**, *73*, 5150.
(21) Preininger, C.; Klimant, I.; Wolfbeis, O. S. *Anal. Chem.* **1994**, *66*, 1841.
(22) Ruffolo, R.; Evans, C. E. B.; Liu, X.-H.; Ni, Y.; Pang, Z.; Park, P.; McWilliams, A. R.; Gu, X.; Lu, X.; Yekta, A.; Winnik, M. A.; Manners, I. *Anal. Chem.* **2000**, *72*, 1894.
(23) Wang, Z.; McWilliams, A. R.; Evans, C. E. B.; Lu, X.; Chung, S.; Winnik, M. A.; Manners, I. *Adv. Funct. Mater.* **2002**, *12*, 415.
(24) Coutant, M. A.; Payra, P.; Dutta, P. K. *Microporous Mesoporous Mater.* **2003**, *60*, 79.
(25) Meier, B.; Werner, T.; Klimant, I.; Wolfbeis, O. S. *Sens. Actuators, B* **1995**, *29*, 240.
(26) Bukowski, R. M.; Ciriminna, R.; Pagliaro, M.; Bright, F. V. *Anal. Chem.* **2005**, *77*, 2670.
(27) Bukowski, R. M.; Davenport, M. D.; Titus, A. H.; Bright, F. V. *Appl. Spectrosc.* **2006**, *60*, 951.
(28) Leventis, N.; Elder, I. A.; Rolison, D. R.; Anderson, M. L.; Merzbacher, C. I. *Chem. Mater.* **1999**, *11*, 2837.
(29) Leventis, N.; Rawashdeh, A.-M. M.; Elder, I. A.; Yang, J.; Dass, A.; Sotiriou-Leventis, C. *Chem. Mater.* **2004**, *16*, 1493.
(30) Murtagh, M. T.; Shahriari, M. R.; Krihak, M. *Chem. Mater.* **1998**, *10*, 3862.
(31) Cheng, Z.; Aspinwall, C. A. *Analyst* **2006**, *131*, 236.
(32) Chu, B. W.-K.; Yam, V. W.-W. *Langmuir* **2006**, *22*, 7437.
(33) Jorge, P. A. S.; Mayeh, M.; Benrashid, R.; Caldas, P.; Santos, J. L.; Farahi, F. *Appl. Opt.* **2006**, *45*, 3760.
(34) Kocincova, A. S.; Borisov, S. M.; Krause, C.; Wolfbeis, O. S. *Anal. Chem.* **2007**, *79*, 8486.
(35) Krenske, D.; Abdo, S.; Van Damme, H.; Cruz, M.; Fripiat, J. J. *J. Phys. Chem.* **1980**, *84*, 2447.
(36) Xiong, X.; Xiao, D.; Choi, M. M. F. *Sens. Actuators, B* **2006**, *117*, 172.

10.1021/ja8075605 CCC: $40.75

the nanoscopic surroundings of each emissive molecule may be different, resulting in heterogeneous emissive sites, and complications can result from the photoinstability of many of the support materials as well as the metal complex itself.[10,14,16,17,21,22,29]

We have recently reported the use of pure nanoporous crystalline solids, such as $[Ru(phen)_3](tfpb)_2$ {tfpb = tetrakis[3,5-bis(trifluoromethyl)phenyl]borate]}, as oxygen sensors.[38] These crystalline materials contain void-space channels that allow the diffusion of oxygen and can eliminate problems of heterogeneity and subsequent inconsistent sensor response.[38] Compared with sensors that use polymeric support materials, sensors based on crystalline solids can have enhanced stability and consistent emissive sites because of the uniformity of the repeat unit in the crystals. Bulky fluorinated counterions like $tfpb^-$ promote the formation of void space within the crystals and allow higher permeability to oxygen.[38]

We recently became aware of another potential method for generating void space within crystalline solids that eliminates the need for large counterions. The Δ and Λ forms of $Ru(phen)_3^{2+}$ can be separated and independently combined with simple counterions to give compounds with different crystalline structures and properties than those of the racemic form.[39] As has been previously observed, pure crystals of the Δ and Λ forms often do not pack as efficiently in the crystal as the racemic mixture, which can lead to a porous structure.[40−42] Herein, we describe the use of microcrystalline samples of simple salts of chiral metal complexes as oxygen sensors. We have separated and studied the pure Δ and Λ forms of $Ru(phen)_3^{2+}$ as the PF_6^- salts and compared the crystalline forms and oxygen-sensing abilities of these chiral salts to racemic $[Ru(phen)_3][PF_6]_2$.

Experimental Section

General Considerations. Racemic $[Ru(phen)_3]Cl_2 \cdot xH_2O$ and potassium antimony tartrate ($K_2[Sb_2\{(+)\text{-tartrate}\}_2] \cdot 3H_2O$) were purchased from Aldrich. Sodium hydroxide (NaOH) and ammonium hexafluorophosphate (NH_4PF_6) were purchased from Mallinckrodt and Aldrich, respectively. Deionized water was used in all cases. All of the reagents were used without further purification. Racemic $[Ru(phen)_3][PF_6]_2$ was synthesized in a previous study by a metathesis reaction of $[Ru(phen)_3]Cl_2 \cdot xH_2O$ with NH_4PF_6.[38]

Optical Resolution of $[Ru(phen)_3]^{2+}$. In general, our procedure follows the method of Nakamura et al.,[39] which is described by the following three equations:

$$\Delta,\Lambda\text{-}[Ru(phen)_3]Cl_2 \xrightarrow[H_2O,\ \Delta]{K_2[Sb_2\{(+)\text{-tartrate}\}_2]} \Lambda\text{-}[Ru(phen)_3][Sb_2\{(+)\text{-tartrate}\}_2](s) + \Delta\text{-}[Ru(phen)_3]^{2+}(aq) + 2Cl^- \quad (1)$$

$$\Lambda\text{-}[Ru(phen)_3][Sb_2\{(+)\text{-tartrate}\}_2](s) \xrightarrow[NH_4PF_6]{0.05\ M\ NaOH} \Lambda\text{-}[Ru(phen)_3][PF_6]_2(s) \quad (2)$$

$$\Delta\text{-}[Ru(phen)_3]^{2+}(aq) \xrightarrow{NH_4PF_6} \Delta\text{-}[Ru(phen)_3][PF_6]_2(s) \quad (3)$$

$[Ru(phen)_3]Cl_2$ (0.356 g, 0.500 mmol) was dissolved in water (24.5 mL).[39] Potassium antimony tartrate (0.334 g, 0.500 mmol) was dissolved with warming in water (12.5 mL) and added to the solution of $[Ru(phen)_3]Cl_2$. An orange solid began precipitating after only a few milliliters of the antimony tartrate solution was added. The solution was heated during the addition of the remaining antimony tartrate solution. Upon completion of the addition of the resolving agent, water (10 mL) was added, and the solution was again heated. As the solution cooled to room temperature overnight, Λ-$[Ru(phen)_3][Sb_2\{(+)\text{-tartrate}\}_2]$ crystallized as an orange solid, which was collected by filtration (0.283 g, 96% yield). The filtrate that contained Δ-$[Ru(phen)_3]^{2+}$ was saved for further reaction.

Λ-$[Ru(phen)_3][PF_6]_2$. Λ-$[Ru(phen)_3][Sb_2\{(+)\text{-tartrate}\}_2]$ (0.1428 g, 0.1213 mmol) was dissolved in 25 mL of hot NaOH solution (0.05 M). Filtration was performed to remove an off-white solid, which was rinsed with an additional 3 mL of 0.05 M NaOH. A 5 mL solution of NH_4PF_6 (1.132 g, 6.945 mmol) was added dropwise and immediately gave a light-orange precipitate of Λ-$[Ru(phen)_3][PF_6]_2$ (0.070 g, 62% yield). The optical purity (enantiomeric excess) of the Λ-$[Ru(phen)_3][PF_6]_2$ was determined by HPLC as 95%. X-ray-quality crystals were grown by recrystallization of the orange solid from an acetonitrile/toluene mixture.

Δ-$[Ru(phen)_3][PF_6]_2$. A 20 mL solution of NH_4PF_6 (2.50 g, 15.4 mmol) was added dropwise to the potassium antimony tartrate filtrate containing Δ-$[Ru(phen)_3]^{2+}$ obtained during the optical resolution of the racemic mixture. Δ-$[Ru(phen)_3][PF_6]_2$ precipitated as an orange solid (0.204 g, 88% yield) with an optical purity (enantiomeric excess) of 99%, as determined by HPLC. X-ray-quality crystals were grown by recrystallization of the orange solid from an acetonitrile/toluene mixture.

HPLC Analysis. The optical purity of the complexes was determined by HPLC on an Agilent 1100 Series liquid chromatograph equipped with a UV-absorbance detector and a Chiralcel OD (4.6 mm i.d. × 25 mm long with 10 μm particles) normal-phase column that was converted to reversed-phase by flushing with acetonitrile/water. The mobile phase was a 50:50 (v/v) mixture of aqueous 0.1 M $NaPF_6$ and acetonitrile with a flow rate of 0.75 mL/min, an injection volume of 50 μL, and a detection wavelength of 400 nm. Representative chromatograms of the pure Δ-, Λ-, and racemic $[Ru(phen)_3][PF_6]_2$ salts are shown in Figure S1 in the Supporting Information.

Spectroscopic and Photophysical Studies. Solid-state UV−vis spectra were acquired from films made from samples used for oxygen sensitivity studies (see below) on a custom-built zirconium oxide attenuated total reflectance (ATR) crystal. The solid-state emission spectra were acquired using an apparatus similar to one described previously.[38] A bifurcated (six-around-one) fiber-optic probe (Ocean Optics) was used to excite the sample and also to collect the emitted light. The excitation light was provided by a 400 nm LED. Spectra were corrected for detector response with an Ocean Optics CCD spectrophotometer that was calibrated with a standard light source.[38] Samples used for oxygen detection were made by dissolving milligram quantities of the Ru complex in acetonitrile and adding the resulting solution to 3 mL of toluene. This resulted in precipitation of microcrystalline samples, which were then centrifuged. These solid samples were removed from the mother liquor and placed either on the tip of a Delrin rod or in a depression in the center of a thermistor (Digi-Key, Allied Electronics) that allowed fast (10 s) heating to ~80 °C. The samples were fitted into a sample compartment that allowed gas flow over the sample. Known percentages of oxygen were made with in-house-built gas-mixing setups using mass-flow control valves. The oxygen concentrations for the Stern−Volmer plots reported here are expressed in terms of mole fraction at the standard

(37) FOXY Fiber-Optic Oxygen Sensors (Ocean Optics, Dunedin, FL).
(38) McGee, K. A.; Veltkamp, D. J.; Marquardt, B. J.; Mann, K. R. *J. Am. Chem. Soc.* **2007**, *129*, 15092.
(39) Nakamura, A.; Sato, T.; Kuroda, R. *Chem. Commun.* **2004**, 2858.
(40) Brock, C. P.; Schweizer, W. B.; Dunitz, J. D. *J. Am. Chem. Soc.* **1991**, *113*, 9811.
(41) Herbstein, F. H. *Crystalline Molecular Complexes and Compounds*; IUCr Monographs on Crystallography *18*, Oxford University Press: Oxford, U.K., 2005; Vol. 1, pp 571−574.
(42) Lancaster, R. W.; Karamertzanis, P. G.; Hulme, A. T.; Tocher, D. A.; Covey, D. F.; Price, S. L. *Chem. Commun.* **2006**, 4921.

atmospheric pressure of Minneapolis−St. Paul, MN (0.97 atm). Data were collected with either Ocean Optics OOIBase32 or custom-written Labview programs that also controlled the oxygen fraction.

Solid-state quantum yields were obtained as previously described.[38] The diffuse reflectance was captured from a "perfectly" scattering surface to give (after integration and correction for instrument response) a quantity proportional to the incident light intensity I_0 (in units of photons/cm^{-1}). In the studies presented here, we used a 1 × 1 cm piece of Fluorilon[43] scattering target. The Fluorilon target is a NIST standard of fused powdered Teflon with a scattering coefficient of >99% across the entire spectral region of interest (350−1000 nm).[43] The surface can be sanded to a reproducible scatter with simple 240 grit sandpaper and reused.[43] The procedure consisted of measuring the diffuse reflectance of the Fluorilon target and then rubbing the freshly grown crystals of interest into the pores of the target with a metal spatula. The light (unabsorbed excitation beam intensity I and emission intensity I_{emit}) from the target with the sample embedded in the surface was then collected. These two measurements allowed the absolute solid-state emission quantum yield to be calculated.[38]

Solid-state lifetime measurements were made as described previously using a pulsed 405 nm LED light source for excitation.[38] Pulsed operation of the LED produced, in addition to the 405 nm light needed for excitation, a long-lived component[44] centered at $\lambda_{max} = 550$ nm that was removed by passing the LED light through a filter.[45] The filtered light pulses were focused onto the end of the fiber-optic inlet leg with a sapphire ball lens.[46] The emitted light (collected through the second fiber-optic leg) was filtered (Kodak #8 Wratten) to remove the remaining LED excitation light and then directed to a Hamamatzu R928 PMT run at 1250 V using the last five dynodes. The PMT detection circuitry was designed by J. C. Scaiano[47] for high momentary currents with fast response times. The time response of this system was better than 1 ns. The PMT signal was read by a sampling digital oscilloscope (Phillips PM 3323). Extensive signal averaging was employed. The oscilloscope was triggered by a logic pulse produced by the LED light source. The weighted plots [$w_i = 1/\sigma_i^2 = 1/I(t)$] of I versus t were fit to single-, double-, or triple-exponential decays (as appropriate) using the Solver in Excel.

Single-Crystal X-ray Crystallography. The crystal structure of Λ-[Ru(phen)$_3$][PF$_6$]$_2$ has been reported previously as a 2:1 acetonitrile/diethyl ether solvate.[48] A crystal of Δ-[Ru(phen)$_3$][PF$_6$]$_2$ grown from an acetonitrile/toluene solvent mixture was attached to a glass capillary fiber and mounted on a Siemens SMART Platform CCD diffractometer for a data collection at 173(2) K using a graphite monochromator and Mo Kα radiation ($\lambda = 0.71073$ Å). An initial set of cell constants was calculated from 93 reflections harvested from three sets of 20 frames such that orthogonal wedges of reciprocal space were surveyed. Final cell constants were calculated from the *xyz* centroids of 3417 strong reflections from the actual data collection. Data were collected to the extent of 1.5 hemispheres and to a resolution of 0.84 Å. Three major sections of frames were collected with 0.30° steps in ω. The intensity data were corrected for absorption and decay using SADABS.[49,50] The space group was determined to be $P4_1$ on the basis of systematic absences and intensity statistics. The absolute structure was determined through confirmation that the space group was $P4_1$ and not $P4_3$ by solving the structure in both space groups and then analyzing the resulting absolute structure parameter [the Flack parameter (x)] in each case. The Flack parameter is near zero when the absolute structure is correct and near one when the structure should be inverted. In this case, when the structure was solved in $P4_1$, $x = 0.0066$ with an estimated standard deviation (ESD) of 0.0386. Solving the structure in $P4_3$ gave $x = 0.9700$ with ESD of 0.0402, indicating a need to reinvert to the space group $P4_1$ and thereby confirming the presence of the Δ enantiomer, as expected. A direct-methods solution provided the positions of most of the non-hydrogen atoms. Full-matrix least-squares/difference Fourier cycles were performed to locate the remaining non-hydrogen atoms. All of the non-hydrogen atoms were refined with anisotropic displacement parameters, and all of the hydrogen atoms were placed in idealized positions and refined as riding atoms with relative isotropic displacement parameters. All of the calculations were performed with the SHELXTL suite of programs.[51] Packing analysis parameters were measured using PLATON/VOID, with more detailed analysis of the void spaces performed with PLATON/CAVITY.[52,53] Pictorial representations of the solvent channels were calculated with edited.res files in Mercury.[54] Details of the refinement are given in Table 1.

Thermogravimetric Analysis. Investigations of mass loss were completed with a PerkinElmer Diamond TG/DTA instrument with an inert nitrogen gas flow. Samples were prepared identically to those used for emission studies and were taken directly from the mother liquor. A 15 min hold time was programmed at the beginning of each run to monitor evaporation of the excess mother liquor to produce dry, solvated samples with masses of 0.5−3 mg. The dry samples were then heated at a rate of 10 °C/min from 20 to 400 °C, and the mass loss was recorded.

Results and Discussion

Resolution of Racemic [Ru(phen)$_3$]$^{2+}$. The racemic mixture of [Ru(phen)$_3$]Cl$_2$ was chemically resolved into the Δ and Λ enantiomers by treatment with potassium antimony tartrate using the method of Nakamura et al.[39] The resulting Δ and Λ antimony tartrate salts were converted to PF$_6^-$ salts in 99% and 95% enantiomeric excess, respectively. Solid samples of the two enantiomers showed no signs of racemization after 9 months. Confirmation of the absolute configurations of these two isomers was obtained by X-ray crystallography.

X-ray Crystallography. Crystals of the Δ enantiomer grown from a combination of acetonitrile and toluene enabled the absolute configuration of the Δ enantiomer to be determined by a single-crystal X-ray structure. The crystal structure of the Λ enantiomer was also previously completed with crystals grown from diethyl ether diffused into acetonitrile.[48] These crystals were reported to undergo facile loss of the interstitial solvent, leading to our modification of the crystal growth procedure by replacing diethyl ether with the higher-boiling toluene. The unit cell parameters and volume of the Δ enantiomer are very similar to those of the Λ enantiomer as reported by Maloney[48] (Table 1), and upon closer investigation, the packing of the ions is almost identical, with helical columns of the chiral complex progressing through the cell. The Δ

(43) Avian Technologies, 116 Newport Rd., Suite 4-6b, New London, NH 03257; http://www.aviantechnologies.com/faq.php (accessed Jan 6, 2009).
(44) Drew, S. M.; Mann, J. E.; Marquardt, B. J.; Mann, K. R. *Sens. Actuators, B* **2004**, *97*, 307.
(45) The filter is a FF01-406/15-25 from Semrock, 3625 Buffalo Road, Rochester, NY 14624.
(46) Araki, T.; Fujisawa, Y.; Hashimoto, M. *Rev. Sci. Instrum.* **1997**, *68*, 1365.
(47) Barbara, P. F. Private communication.
(48) Maloney, D. J.; MacDonnell, F. M. *Acta Crystallogr., Sect. C: Cryst. Struct. Commun.* **1997**, *53*, 705.
(49) Blessing, R. H. *Acta Crystallogr., Sect. A: Found. Crystallogr.* **1995**, *51*, 33.
(50) Sheldrick, G. M. *SADABS*, version 2.10; 2002; University of Göttingen, Germany.
(51) *SHELXTL*, version 6.12; Bruker AXS: Madison, WI, 2001.
(52) Spek, A. L. *J. Appl. Crystallogr.* **2003**, *36*, 7.
(53) Spek, A. L. *PLATON*; Utrecht University: Utrecht, The Netherlands, 2005.
(54) Bruno, I. J.; Cole, J. C.; Edgington, P. R.; Kessler, M.; Macrae, C. F.; McCabe, P.; Pearson, J.; Taylor, R. *Acta Crystallogr., Sect. B: Struct. Sci.* **2002**, *58*, 389.

Table 1. Crystallographic Data and Refinement Parameters

compound	2Δ-[Ru(phen)$_3$][PF$_6$]$_2$·2CH$_3$CN·toluene	2Λ-[Ru(phen)$_3$][PF$_6$]$_2$·2CH$_3$CN·Et$_2$O[a]
empirical formula	$C_{83}H_{62}F_{24}N_{14}P_4Ru_2$	$C_{80}H_{64}F_{24}N_{14}OP_4Ru_2$
crystal color, morphology	orange, needle	orange, parallelepiped
crystal system	tetragonal	tetragonal
space group	$P4_1$	$P4_3$
a (Å)	25.5737(9)	25.372(1)
b (Å)	25.5737(9)	25.372(1)
c (Å)	12.5736(9)	12.726(2)
α (deg)	90	90
β (deg)	90	90
γ (deg)	90	90
V (Å^3)	8223.3(7)	8192.2(2)
Z	4	4
formula weight (g/mol)	2037.49	2019.48
D_{calcd} (g/cm^3)	1.646	1.637
T (K)	173(2)	183(2)
absorption coefficient (mm^{-1})	0.556	0.558
F(000)	4088	4056
θ range (deg)	0.80 to 25.04	5.08 to 16.48
index ranges	$-22 \le h \le 30$	$-30 \le h \le 30$
	$-30 \le k \le 26$	$-30 \le k \le 30$
	$-14 \le l \le 14$	$-15 \le l \le 15$
reflections collected	38214	15846
independent reflections	14398 ($R_{int} = 0.0849$)	14413 ($R_{int} = 0.030$)
weighting factors a, b [b]	0.0873, 0.0	
transmission max, min	0.9835, 0.7686	0.774, 0.695
data, restraints, parameters	14398, 58, 1130	14413, 0, 1124
R_1, wR_2 [$I > 2\sigma(I)$]	0.0730, 0.1549	0.063, 0.160
R_1, wR_2 (all data)	0.1209, 0.1755	
GOF	1.027	1.075
largest diff. peak, hole (e/Å^3)	0.731, −0.502	0.66, −0.55

[a] Previously determined (see ref 48). [b] $w = [\sigma^2(F_o^2) + (aP)^2 + (bP)]^{-1}$, where $P = (F_o^2 + 2F_c^2)/3$.

enantiomer has two formula units in the asymmetric unit, with the Ru cations related by a pseudotwofold screw axis, as is the case in the structure of a different solvate of the Λ enantiomer.[48]

The cations contain pseudooctahedral Ru. The average Ru−N bond length (2.066 Å) and angles between least-squares planes made from the ligands (82.4, 88.8, and 81.5° for Ru1 and 86.0, 85.0, and 85.9° for Ru2) correlate well with the literature values reported for the Λ enantiomer (average Ru−N distance of 2.067 Å; angles of 80, 86, and 90° for Ru1 and 86, 90, and 87° for Ru2).[48] The Δ enantiomer crystallizes as a solvate with two acetonitrile molecules and one toluene per asymmetric unit. On the basis of the close similarity of our structure with the literature structure for the Λ enantiomer, we make the assumption that Λ-[Ru(phen)$_3$](PF$_6$)$_2$ crystallized from acetonitrile and toluene would have the same structure with two cocrystallized acetonitrile molecules and one toluene.

Examination of the molecular packing of the structures of the Δ and Λ enantiomers shows a narrow channel of open space running though the structure as well as another larger channel partially occupied by the acetonitrile and toluene solvent molecules (Figure 1, top). One can envision that the loss of some of this cocrystallized solvent would significantly increase the amount of void space accessible to small molecules. The channels observed in the chiral structures are not present in the structure of racemic [Ru(phen)$_3$](PF$_6$)$_2$,[55] which contains no solvent molecules and a much smaller amount of open space in the form of isolated voids (Figure 1, bottom). The channels observed in the chiral structures could allow diffusion of small molecules such as oxygen into and out of these crystals, allowing them to be used as sensors. Conversely, the presence of small isolated voids in the racemic crystal may not enable diffusion of oxygen to the interior; hence, we expect poor oxygen sensing in this case (see below).

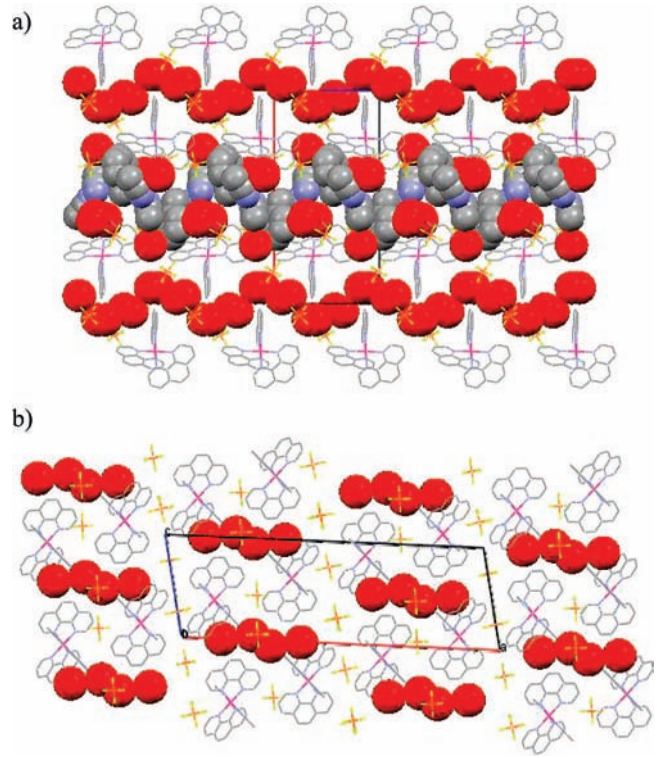

Figure 1. Packing diagrams of crystal structures, viewed down the b axis, of (a) Δ-[Ru(phen)$_3$](PF$_6$)$_2$·toluene·2CH$_3$CN and (b) racemic [Ru(phen)$_3$](PF$_6$)$_2$.[55] The red spheres, which have an average diameter of ∼2.4 Å, represent open space.

(55) Breu, J.; Stoll, A. J. *Acta Crystallogr., Sect. C: Cryst. Struct. Commun.* **1996**, *52*, 1174.

Table 2. Spectroscopic and Photophysical Data

	absorbance λ_{max} (nm)	emission λ_{max} (nm)	$\tau_{M,nitrogen}$ (ns)	$\phi_{nitrogen}$	$\Delta\phi/\phi_0$
Δ-[Ru(phen)$_3$](PF$_6$)$_2$	465	599	462	0.05(2)	0.36(2)
Λ-[Ru(phen)$_3$](PF$_6$)$_2$	466	601	464	0.05(2)	0.33(2)
Δ,Λ-[Ru(phen)$_3$](PF$_6$)$_2$	459	590	392	0.04(2)	0.05(2)

Thermogravimetric Analysis. Samples prepared identically to those analyzed for oxygen sensitivity were investigated by thermal gravimetric analysis (TGA) (see Figure S5 in the Supporting Information). A gradual loss of mass occurred upon heating, with three ill-defined inflection points. The first inflection point, at 40 °C, corresponds to loss of 0.25 acetonitrile molecules per Ru, which we believe leaves from the smaller channel in the crystal structure. We believe that the loss of this portion of the solvent also occurs readily at room temperature in air for bulk samples and was not present in the lattice during the crystallographic data collection or at the beginning of the oxygen sensitivity studies. The next two inflection points occur at ~60 and 80 °C and correspond to the loss of 0.5 acetonitriles per Ru at each point. A further mass loss of 0.5 toluene molecules per Ru occurs as the temperature increases to ~140 °C, after which the mass loss is minimal until the temperature reaches 380 °C, where the samples undergo decomposition. The total mass lost between 40 and 140 °C corresponds to 1.0 acetonitrile molecule and 0.5 toluene molecules per [Ru(phen)$_3$](PF$_6$)$_2$, in excellent agreement with the crystal structure. Under the constant heating rate conditions of the TGA experiment, the acetonitrile molecules in the structure are lost in 8−9 min between 25 and 80 °C.

Photophysical Studies. The room-temperature solid-state absorption and emission spectra for the three salts {racemic, pure Δ-, and pure Λ-[Ru(phen)$_3$](PF$_6$)$_2$} were collected under nitrogen. The λ_{max} values [along with absolute emission quantum yields ($\phi_{nitrogen}$) and mean lifetimes ($\tau_{M,nitrogen}$)] are reported in Table 2. The respective λ_{max} values for absorption and emission for the two pure enantiomers are nearly identical and are red-shifted (by ~6 nm for absorption and 10 nm for emission) relative to those of the racemic compound, likely as a result of interactions between the cations and solvent molecules in the pure chiral compounds that are not present in the racemic crystals. This pattern of physical property results (pure Δ and pure Λ enantiomers the same, racemic different) is expected and was confirmed for all of the solid-state measurements we report herein.

Solid-state absolute emission quantum yields were collected for the racemic and pure Δ and Λ enantiomer [Ru(phen)$_3$](PF$_6$)$_2$ salts as described previously[38] using a Fluorilon scattering target.[43] The quantum yields were found to be very dependent on the treatment of the solids,[38] with significantly lower values obtained from measurements on solids that had been evaporated from acetonitrile containing no toluene. The values reported in Table 2 were obtained for 10−20 mg samples that had been dissolved in a small amount of acetonitrile (0.05 mL) and added to toluene (3 mL), resulting in a crystalline precipitate.

Emission Intensity Quenching Studies. Because of the presence of void space in their crystalline lattices, both the Δ and Λ enantiomers were examined for their utility as oxygen sensors. Additionally, for comparison, racemic [Ru(phen)$_3$](PF$_6$)$_2$ was also investigated. The quenching effect of air on the solid-state emission was examined by emission intensity measurements under nitrogen and air (Figure 2).

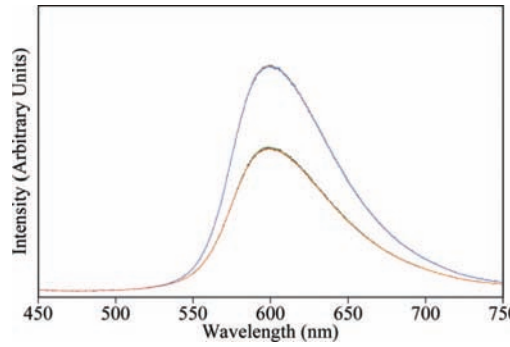

Figure 2. Emission spectra of solid Δ-[Ru(phen)$_3$](PF$_6$)$_2$ under nitrogen (blue) and under air (red), showing the quenching of the emission in the presence of oxygen and the reversibility of the sensor. Each exposure level contains 5 overlaid spectra collected in an alternating fashion.

The extent of emission quenching in the presence of air was quantified using the integrated intensities of the emission to give a fraction of emission quenched, according to eq 4:

$$\text{fraction of integrated emission quenched} = \frac{I_0 - I}{I_0} = \frac{\Delta I}{I_0} = \frac{\Delta\phi}{\phi_0} \quad (4)$$

where I_0 is the normal Stern−Volmer (SV) intensity with no quencher present and I is the SV intensity with air present.

The solid-state emission from each pure enantiomer was reversibly quenched in the presence of air compared with the emission in nitrogen (Figure 2). The fractions of emission quenched were 0.36(2) and 0.33(2) for the Δ and Λ enantiomers, respectively, after conditioning (see below). In contrast, the racemic salt gave a very small fraction quenched [0.05(2)]. The sensitivities of these chiral crystalline solids to oxygen are similar to those in racemic salts with significant void space that we have previously studied, such as [Ru(phen)$_3$](tfpb)$_2$, which exhibits a fraction of emission quenched of 0.354 in air.[38] Immediately after samples of the enantiomers were removed from the crystallization mixture and prepared for measurements, the sensing behavior was less strong than in the steady-state case reported in Table 2, with fractions of emission quenched under air of 0.15(2). The Table 2 values were obtained when samples were conditioned either under a flow of nitrogen for long times (days) or heated in several 10 s increments on a thermistor to more rapidly remove a portion of the acetonitrile of crystallization. The emission quenching of the freshly prepared samples in the presence of air increases, resulting in a stable sensor, when a portion of the loosely held solvent of crystallization is released. We believe that loss of 0.5 equiv of acetonitrile per Ru (one acetonitrile per asymmetric unit, which is half of the acetonitrile present) results in the generation of an equivalent amount of void space and a stable sensing state.

The oxygen-sensing ability of the chiral salts correlates well with the fraction of emission quenched found for crystalline Ru salts previously studied as oxygen sensors (Figure 3). The fraction quenched for the preconditioned state, 0.15(2), fits on the correlation line in Figure 3 assuming that oxygen may only diffuse in the small channel of the structure. The mild thermistor heating results in loss of half of the cocrystallized acetonitrile, yielding additional void space and a higher fraction quenched, again in good agreement with the previous correlation. Additional heating of the sample results in further solvent loss and diminished sensitivity to oxygen, most likely due to the collapse of the structure and loss of crystallinity. It is worthy of note that occasionally a solvation state that was more sensitive to

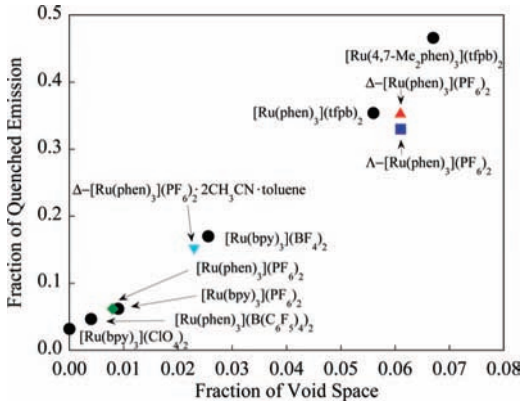

Figure 3. Comparison of the Δ-[Ru(phen)$_3$](PF$_6$)$_2$ (▲) and Λ-[Ru(phen)$_3$](PF$_6$)$_2$ (■) salts to the correlation of the fraction of emission quenched in the presence of air with the fraction of void space present for several Ru(bpy)$_3^{2+}$ and Ru(phen)$_3^{2+}$ salts, including racemic [Ru(phen)$_3$](PF$_6$)$_2$ (◆). The fraction of quenched emission immediately after samples of the enantiomers were removed from the crystallization mixture (▼) is also shown.

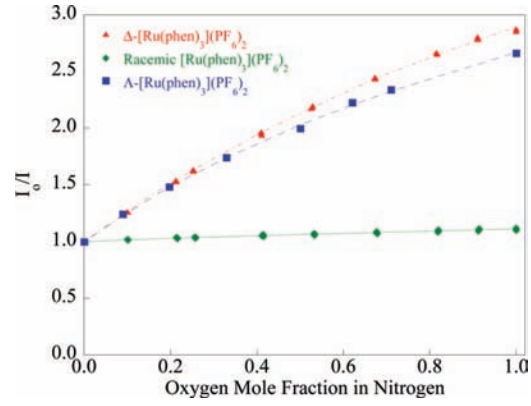

Figure 4. Stern−Volmer intensity plots (I_0/I vs oxygen mole fraction) for Δ-[Ru(phen)$_3$](PF$_6$)$_2$ (▲), Λ-[Ru(phen)$_3$](PF$_6$)$_2$ (■), and the racemic mixture (◆). The two-site model fits for Δ-[Ru(phen)$_3$](PF$_6$)$_2$ (dotted-dashed line) and Λ-[Ru(phen)$_3$](PF$_6$)$_2$ (dashed line) and the linear fit for the racemic mixture (solid line) are included.

air was observed. These samples exhibited fractions of emission quenched on the order of 0.41−0.45. We believe that this state results from a slower heating rate, but repeated attempts to produce this state on demand were unsuccessful.

The quenching behavior of these salts was investigated further by using mass-flow control valves to produce specific concentrations of oxygen in nitrogen. Emission intensity measurements for microcrystalline samples of the two pure enantiomers as well as of racemic [Ru(phen)$_3$](PF$_6$)$_2$ were collected and are displayed in Figure 4 as SV plots (I_0/I vs mole fraction of oxygen in nitrogen at atmospheric pressure).

The importance of void space as a structural feature enabling excited-state quenching by molecular oxygen in these crystalline materials is obvious. The Δ and Λ enantiomers, which exhibit void-space channels and solvent molecules in their crystalline lattices, allow the diffusion of oxygen into the solid and subsequent quenching of the emission of the complex, while the racemic [Ru(phen)$_3$](PF$_6$)$_2$ salt, with smaller isolated voids, does not allow significant oxygen diffusion and exhibits very little quenching. The curved SV plots seen for the Δ and Λ enantiomers can be fit to a two-site SV model according to eq 5:

$$\frac{I_0}{I} = \left(\frac{f_1}{1 + K_{SV1}[O_2]} + \frac{f_2}{1 + K_{SV2}[O_2]} \right)^{-1} \qquad (5)$$

where I_0 is the normal SV intensity with no quencher present, I is the SV intensity with some concentration of O_2 present, the f_i are the fractional contributions to the unquenched emission ($f_1 + f_2 = 1$), K_{SV1} and K_{SV2} are the different SV quenching constants, and $[O_2]$ is the concentration of oxygen. In an ideal system with only dynamic quenching of a single emitting site ($f_2 = 0$), the SV quenching gives a linear relationship between I_0/I and the concentration of oxygen. The curvature of the pure-enantiomer SV plots indicates more complicated behavior. For the Δ isomer, the two-site model results in a fit where one emitting species has an SV constant (K_{SV1}) of 3.31 and a fractional contribution to the total emission (f_1) of 0.85, while the second emitting species has $K_{SV2} \approx 0$ and $f_2 = 1 - f_1 = 0.15$. Similar results are presented in Table 3 for the Λ isomer. The simulated SV plots are in excellent agreement with the experimental intensity data for the Δ and Λ enantiomers (shown in Figure 4 as well as in Figures S2 and S3, respectively, in the Supporting Information). In comparison, the racemic salt exhibits linear SV quenching behavior ($f_2 \approx 0$) with a very small K_{SV} value of ∼0.110.

Table 3. Parameters for the Fit of the Intensity Data for the Pure Δ and Λ Enantiomers and the Racemic Mixture to the Two-Site SV Model

	Δ-[Ru(phen)$_3$](PF$_6$)$_2$	Λ-[Ru(phen)$_3$](PF$_6$)$_2$	Δ,Λ-[Ru(phen)$_3$](PF$_6$)$_2$
K_{SV1}	3.305	3.513	0.110
f_1	0.852	0.782	1.00
K_{SV2}	0	0.0812	0
f_2	0.148	0.218	0

Table 4. Emission Decay Lifetimes and Fractional Components for 0 and 100% Oxygen for the Chiral and Racemic Salts

	Δ-[Ru(phen)$_3$](PF$_6$)$_2$		Λ-[Ru(phen)$_3$](PF$_6$)$_2$		Δ,Λ-[Ru(phen)$_3$](PF$_6$)$_2$	
	0% O_2	100% O_2	0% O_2	100% O_2	0% O_2	100% O_2
α_a	0.448	0.711	0.510	0.683	0.882	0.408
τ_a (ns)	207	65.8	206	89.7	320	183
α_b	0.535	0.283	0.455	0.304	0.114	0.583
τ_b (ns)	631	300	664	284	765	384
α_c	0.0171	0.00606	0.0354	0.0129	0.00360	0.00887
τ_c (μs)	1.88	1.96	1.99	2.12	6.30	2.55
τ_M (μs)	0.462	0.143	0.464	0.175	0.392	0.321

Emission Lifetime Studies. Solid-state emission lifetime data for the pure Δ and Λ enantiomers as well as for the racemic salt were collected and are summarized with other spectroscopic and photophysical data in Table 4. Emission decay data were obtained for samples under a nitrogen atmosphere and various concentrations of oxygen. Single- and double-exponential modeling of the emission decay data provided inadequate fits in each case. The emission decay data for all of the complexes at all oxygen concentrations were satisfactorily modeled using three weighted exponentials. Data for both pure enantiomers were modeled independently with very similar sets of parameters. Data for pure nitrogen and pure oxygen are given in Table 4. In each case, the emission decay is dominated by two decays (∼630 and 205 ns under nitrogen) that are significantly quenched to differing extents in the presence of oxygen. The inclusion of a very small amount (0.05−3%) of a long-lived (∼2 μs) third component that is not quenched in the presence of oxygen was needed to adequately model the time response of the decay. It is not known whether this long-lived component, which is

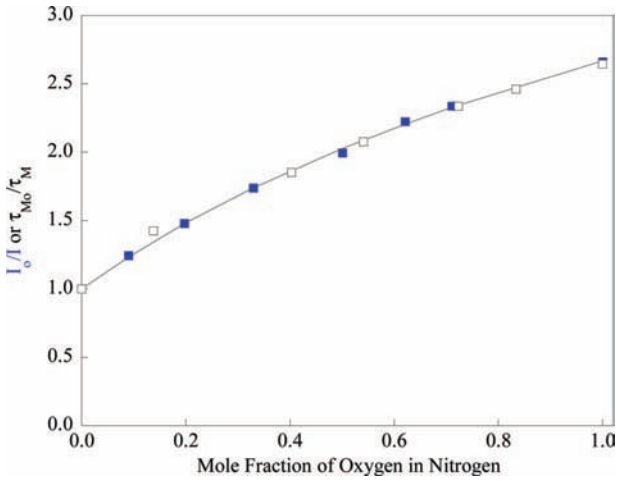

Figure 5. Overlaid SV intensity (■) and pre-exponential weighted mean lifetime (□) data for Λ-[Ru(phen)$_3$](PF$_6$)$_2$, including the two-site model fit for the intensity data (solid line).

common to all of the samples, arises from an impurity or is an instrumental artifact.

The pre-exponential weighted mean lifetime, τ_M, as defined by Carraway and Demas[56,57] was used to compare the intensity and lifetime quenching data for evidence of static quenching:

$$\tau_M = \frac{\sum \alpha_i \tau_i}{\sum \alpha_i} \quad (6)$$

This weighted lifetime is calculated from the triple-exponential fit of the intensity decay curve, where the α_i are the normalized pre-exponential factors and the τ_i are the observed lifetimes. If only dynamic (diffusional) quenching occurs, then

$$\frac{\tau_{M,0}}{\tau_M} = \frac{I_0}{I} \quad (7)$$

and an SV plot using $\tau_{M,0}/\tau_M$ should closely match the SV intensity plot. The SV weighted emission lifetime plots for the Δ enantiomer and especially the Λ enantiomer (Figure 5) match the respective intensity plots quite well, ruling out any significant contribution of static quenching in the mechanism. The nearly identical behavior of the two chiral salts suggests that the underlying photophysical kinetics in the pure solid Δ and Λ enantiomers are virtually identical. It is interesting that the lifetime data required more fitting parameters than the intensity data would suggest; this situation has been discussed by Mills[18] and Demas and co-workers.[57−59] As Demas and co-workers have suggested for oxygen quenching of ruthenium polypyridyls in polymer matrices,[57] the parameters from the lifetime fitting are not necessarily directly interpretable but are more likely composites of the real parameters that result from a more complicated photophysical mechanism. Further efforts are underway to derive an underlying photophysical model that involves, for example, energy migration between the two crystallographically distinct sites with different oxygen quenching rates.

Conclusions

[Ru(phen)$_3$]Cl$_2$ was chemically resolved into Δ and Λ enantiomers, which were then metathesized to the PF_6^- salts. The pure Δ-[Ru(phen)$_3$](PF$_6$)$_2$ and Λ-[Ru(phen)$_3$](PF$_6$)$_2$ salts exhibit the same crystalline structure, through which run narrow channels of void space as well as larger channels occupied by cocrystallized solvent molecules. In contrast, crystals of the racemic mixture contain a much smaller amount of open space in the form of isolated voids, which do not allow significant oxygen diffusion. The chiral salts exhibit increased sensitivity to oxygen with mild heating; thermogravimetric experiments indicate the loss of acetonitrile, which increases the fraction of void space in the crystals. The SV quenching behavior of these materials correlates with the volume accessible to oxygen: the chiral salts exhibit significant quenching with increasing oxygen concentration, while the racemic salt exhibits very little quenching. These systems demonstrate that chiral packing offers an alternative to the bulky fluorinated counterions used previously to generate the void-space channels within crystalline solids necessary for oxygen diffusion and detection.

Acknowledgment. This work was supported by the Center for Analytical Chemistry at the University of Washington and the Initiative for Renewable Energy and the Environment at the University of Minnesota. Also, K.A.M. acknowledges the University of Minnesota for financial support in the form of a Doctoral Dissertation Fellowship. The authors acknowledge the University of Minnesota X-ray crystallography laboratory. Additionally, K.A.M. thanks Conor S. Smith for writing Labview programs for computer control of the mass-flow control valves used in this study, Xiaoli Wang and Alicia A. Peterson for assistance with HPLC, and Peter W. Carr for providing the chiral HPLC column.

Supporting Information Available: Atomic coordinates, bond lengths, and angles for the crystal structure of the Δ enantiomer (CIF); chiral HPLC chromatograms, lifetime intensity plots, lifetime SV plots, a TGA mass loss plot, and intensity SV plots with two-site model fits for the Δ and Λ enantiomers. This material is available free of charge via the Internet at http://pubs.acs.org.

JA8075605

(56) Carraway, E. R.; Demas, J. N.; DeGraff, B. A. *Anal. Chem.* **1991**, *63*, 332.
(57) Carraway, E. R.; Demas, J. N.; DeGraff, B. A.; Bacon, J. R. *Anal. Chem.* **1991**, *63*, 337.
(58) Demas, J. N.; DeGraff, B. A. *Sens. Actuators, B* **1993**, *11*, 35.
(59) Klimant, I.; Wolfbeis, O. S. *Anal. Chem.* **1995**, *67*, 3160.